Immunity, Vol. 20, 219–230, February, 2004, Copyright ©2004 by Cell Press

Human CD8+ T Cells Store RANTES in a Unique Secretory Compartment and Release It Rapidly after TcR Stimulation

Marta Catalfamo,[1] Tatiana Karpova,[2] James McNally,[2] Sylvain V. Costes,[3] Stephen J. Lockett,[3] Erik Bos,[4] Peter J. Peters,[4] and Pierre A. Henkart[1,*]

[1]Experimental Immunology Branch
[2]Laboratory of Receptor Biology and Gene Expression
National Cancer Institute
National Institutes of Health
Bethesda, Maryland 20892
[3]Microscopy and Image Analysis Laboratory
National Cancer Institute-SAIC
Frederick, Maryland 21702
[4]The Netherlands Cancer Institute
1066 CX Amsterdam
Netherlands

Summary

The chemokine RANTES is secreted rapidly after activation of human CD8+ T cells, with a cycloheximide-resistant burst during the first hour. This pattern was observed in purified memory and effector phenotype CD8+ cells from blood as well as in blasts. In contrast, secretion of other chemokines and interferon-γ by these cells was sensitive to cycloheximide and detectable only after a lag. Immunofluorescence microscopy of CD8+ memory and effector cells and blasts showed RANTES present in intracellular vesicles that do not significantly colocalize with cytotoxic granule markers or other markers of defined cytoplasmic compartments. Immunoelectron microscopy confirmed that RANTES is stored in small vesicles distinct from the lysosomal secretory granules. RANTES+ vesicles polarize rapidly in response to TcR engagement and are more rapidly depleted from the cytoplasm. These results show that CD8+ T cells have two distinct TcR-regulated secretory compartments characterized by different mobilization kinetics, effector molecules, and biological function.

Introduction

T lymphocytes function by secreting protein mediators that regulate the activities of other cells. This secretion occurs via two pathways previously defined by cell biologists: the "constitutive" secretory pathway, in which newly synthesized proteins are immediately released by exocytosis of small vesicles after Golgi processing; and the "regulated" secretory pathway, in which protein mediators are stored in intracellular granules until TcR engagement signals their exocytosis (Kelly, 1985). In lymphocytes, the latter pathway has been closely associated with cytotoxic function, and the exocytosis of lysosomal granules containing perforin and granzymes has been clearly demonstrated to be a major effector pathway of cytotoxicity both in vitro and in vivo (Henkart, 1994). TcR-stimulated secretion of γ-interferon is dependent on newly synthesized protein (Fortier et al., 1989), and this constitutive secretory pathway is used by cytokines secreted by both CD8+ and CD4+ T cells.

Reports of chemokine secretion via granule exocytosis in NK cells and cloned CTL lines presented clear evidence that the regulated secretory pathway may not be devoted exclusively to cytotoxicity in lymphocytes (Greenberg et al., 1986; Wagner et al., 1998). Chemokines are recognized as major mediators of inflammation in vivo (Zlotnik and Yoshie, 2000), and inflammatory chemokines, including MIP-1α (CCL3), MIP-1β (CCL4), and RANTES (CCL5), recruit receptor-bearing leukocytes selectively to sites of injury or pathogens (Sallusto et al., 2000). Both CD4+ and CD8+ T cells secrete a significant level of chemokines in inflammatory situations, creating a positive feedback loop for lymphocyte infiltration (Conlon et al., 1995; Robinson et al., 1995). Although TcR-induced chemokine gene transcription has often been assumed to implicate the constitutive secretory pathway, the role of the regulated secretory pathway in T cell chemokine secretion has not been systematically addressed. In particular, it has been unclear whether the regulated secretion described in cloned CTL cell lines is representative of lymphocytes in vivo.

In the current study, we have assessed the role of the regulated pathway of chemokine secretion by human naive, memory, and effector CD8+ T cell subsets and in CD8+ blasts. We show that RANTES is stored intracellularly postnaive CD8+ T cells and is secreted by both regulated and constitutive pathways after activation. Most intracellular RANTES is stored in a distinct compartment that we refer to as RANTES storage vesicles (RSV), which are functionally and structurally distinct from the major secretory lysosomal granules containing perforin and granzymes. After TcR ligation, RSV polarize and are exocytosed more rapidly and efficiently than the lysosomal granules.

Results

CD8+ T Cells Rapidly Secrete RANTES in the Absence of Protein Synthesis

CD8+ T cell subsets purified from normal human blood based on CD45RA and CD27 phenotype were examined for chemokine and IFN-γ secretion after stimulation by PMA and ionomycin. As shown in Figure 1A, substantial RANTES was detected by ELISA assay in the supernatants of effector and memory phenotype cells within 30 min, while naive CD8+ T cells showed no detectable levels at any time. MIP-1β and IFN-γ were detectable in memory cell supernatants by parallel assays but only after several hours of incubation, and neither was detectable in the supernatants of activated naive phenotype cells. In other experiments, MIP-1β was secreted by the CD8+ effector subset similar to that shown for the memory cells (data not shown).

To examine the role of new protein synthesis on this

*Correspondence: henkartp@mail.nih.gov

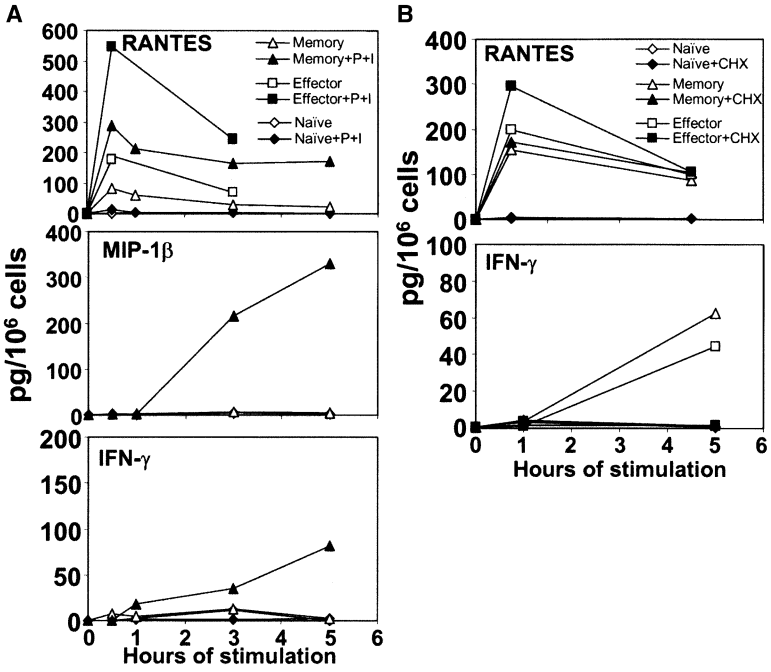

Figure 1. Activation-Induced Chemokine and Interferon-γ Secretion by Human Blood CD8+ T Cell Subsets

(A) CD8+ T cell subsets were purified from blood by flow cytometry based on CD27 and CD45RA phenotype and cultured with and without PMA and ionomycin stimulation. The supernatants were analyzed for chemokines and IFN-γ by ELISA assay at the indicated times. RANTES was analyzed in naive, memory, and effector subsets, while in this experiment MIP-1β and IFN-γ were analyzed only in naive and memory subsets.

(B) In a similar experiment, the effect of cycloheximide preincubation on PMA and ionomycin-induced secretion of RANTES and IFN-γ was examined. The low values for naive interferon-γ secretion are obscured by the cycloheximide points.

secretion, T cells were preincubated with cycloheximide prior to stimulation (Figure 1B). RANTES secretion in both memory and effector phenotype cells was minimally affected by cycloheximide, while IFN-γ secretion (detected in this experiment in both memory and effector subpopulations) was totally blocked under these conditions.

To examine RANTES secretion in CD8+ T cells in which TcR engagement leads to measurable granule exocytosis, we stimulated CD8+ T cell blasts with plate-bound anti-CD3 and CD28 mAbs (Figure 2). RANTES secretion was again detected within 30 min of stimulation, with little further increase after 1 hr (Figure 2A). This secretion showed no significant inhibition with cycloheximide or emetine preincubation. Secretion of the lysosomal enzyme β-hexosaminidase, a marker for granule exocytosis (Winslow and Austen, 1982), was detectable after 30 min, continued to increase beyond 1 hr, and was insensitive to cycloheximide. MIP-1α, a second inflammatory chemokine reported in granules of cloned CTL (Wagner et al., 1998), was barely detectable in supernatants within the first hour. Incubations of 3 hr allowed detection of other secreted mediators and confirmed that both early RANTES secretion and degranulation are resistant to cycloheximide, emetine (data not shown), and brefeldin A, an inhibitor of the ARF1 exchange factor, which is critical for the integrity of the Golgi complex (Figure 2B). As found in resting CD8+ T cells, IFN-γ secretion was undetectable at early times but was clearly detectable at 3 hr. This secretion was totally blocked by cycloheximide, emetine (data not shown), and brefeldin A. MIP-1β showed somewhat more rapid secretion, which was also blocked effectively by cycloheximide and brefeldin A. MIP-1α secretion showed an identical pattern but never approached the supernatant level of RANTES (data not shown).

The above results indicated that, at early times after activation, RANTES secretion by CD8+ T cells is similar to granule exocytosis in that it shows no kinetic lag and is resistant to inhibitors of the constitutive secretory pathway. However, there were also consistent differences between the secretion of RANTES and granule mediators. RANTES secretion plateaued or even decreased after 30 min as opposed to the continued increase in degranulation in all three CD8+ T cell systems measured, while release of the granule enzyme in the blasts continued for 3 to 4 hr before plateauing (Figures 1 and 2, and data not shown). Another difference became apparent when, in addition to supernatant release, we also measured the total RANTES in the cells by assaying Triton lysates (in parallel to measurements of the total β-hexosaminidase for the degranulation assay). These experiments showed that at 1 hr, over 50% of the total RANTES detectable in lysates of CD8+ memory, effector, and blasts was secreted, as opposed to 10%–20% of the total β-hexosaminidase seen in blasts (Figure 2). A final difference was that RANTES consistently showed a higher level of unstimulated basal secretion than β-hexosaminidase.

Intracellular RANTES in CD8+ T Cells

The above secretion experiments strongly suggest that memory, effector, and blast CD8+ T cells contain stored RANTES that can be secreted by activation. To quantitate intracellular RANTES expression and compare it to the cytolytic granules, we carried out flow cytometry of permeabilized subpopulations of resting CD8+ T cells previously surface stained with antibodies to CD45RA and CD27 in order to correlate intracellular expression with surface phenotype (Figure 3). Naive phenotype CD8+ cells (CD45RA+CD27+) contain no significant intracellular RANTES or granzyme B. In contrast, memory phenotype CD8+ T cells (CD45RA−CD27+) contain clearly detectable intracellular RANTES-positive vesi-

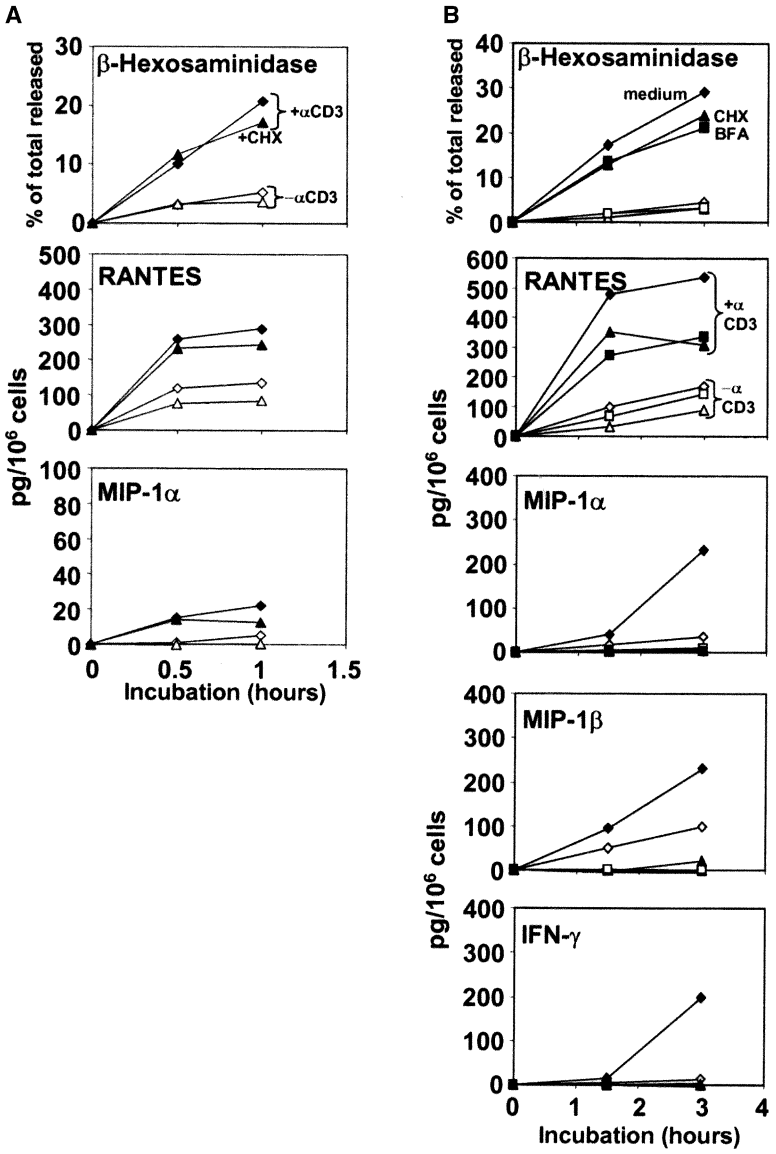

Figure 2. Activation-Induced Secretion by Human CD8+ T Cell Blasts

Purified CD8+ T cell blasts from short-term cultures were stimulated with plate-bound anti-CD3 + anti-CD28. The supernatants were collected at the indicated times and analyzed for the indicated mediators (β-hexosaminidase by enzymatic activity and chemokines and IFN-γ by ELISA). Cells were pretreated with cycloheximide (CHX, 7.5 μg/ml) as indicated to block protein biosynthesis. Data is plotted as the percentage secreted compared to the Triton X-100 lysate total for β-hexosaminidase and as absolute supernatant concentrations secreted for chemokines, although lysates were also analyzed in the latter cases. The experiment in (B) was analyzed at 3 hr after activation to allow detection of additional mediators as indicated and included pretreatment with Brefeldin A (BFA, 5 μg/ml) as well as CHX to inhibit the constitutive secretory pathway.

cles in a relatively homogeneous distribution, as well as vesicular granzyme B in a small subpopulation. The effector subpopulation (CD45RA+CD27−), which contains high levels of vesicular granzyme B, also contains vesicular RANTES at levels comparable to the memory phenotype cells.

Intracellular RANTES expression was also examined in light of the proposed subdivision of CD45RA− human memory CD8+ T cells into two subsets based on the expression of CCR7 (Sallusto et al., 1999). Flow cytometric analysis similar to that described above was carried out (Figure 3B), revealing that vesicular RANTES expression in the CD45RA−CCR7+ "central memory" CD8+ cells was somewhat heterogeneous, containing a subpopulation with undetectable RANTES expression similar to naive CD8+ cells. However, most of this memory subpopulation expressed clearly detectable vesicular RANTES at a level similar to the more homogeneous expression in the "effector memory" and effector subpopulations. In agreement with the results using CD27 phenotyping, vesicular granzyme B expression was very low except in the effector subpopulation, where most cells showed good expression.

RANTES Intracellular Localization in CD8+ T Cells

Given the above results that RANTES is expressed in cytoplasmic vesicles in memory and effector CD8+ lymphocytes, we purified CD8+ subpopulations by cell sorting and examined permeabilized cells by two color fluorescence microscopy, using a high-resolution deconvolution digital image analysis (Figure 3C). RANTES (red stain) was not detectable in CD45RA+CD27− naive cells, as predicted from flow cytometry. Both memory and effector phenotype showed that intracellular RANTES is distributed quite symmetrically throughout the cells in defined vesicular compartments. Based on the report that RANTES is expressed in granules in cloned CTL (Wagner et al., 1998), we costained with the granule marker cathepsin B. We were surprised to find minimal colocalization of the RANTES+ vesicles with

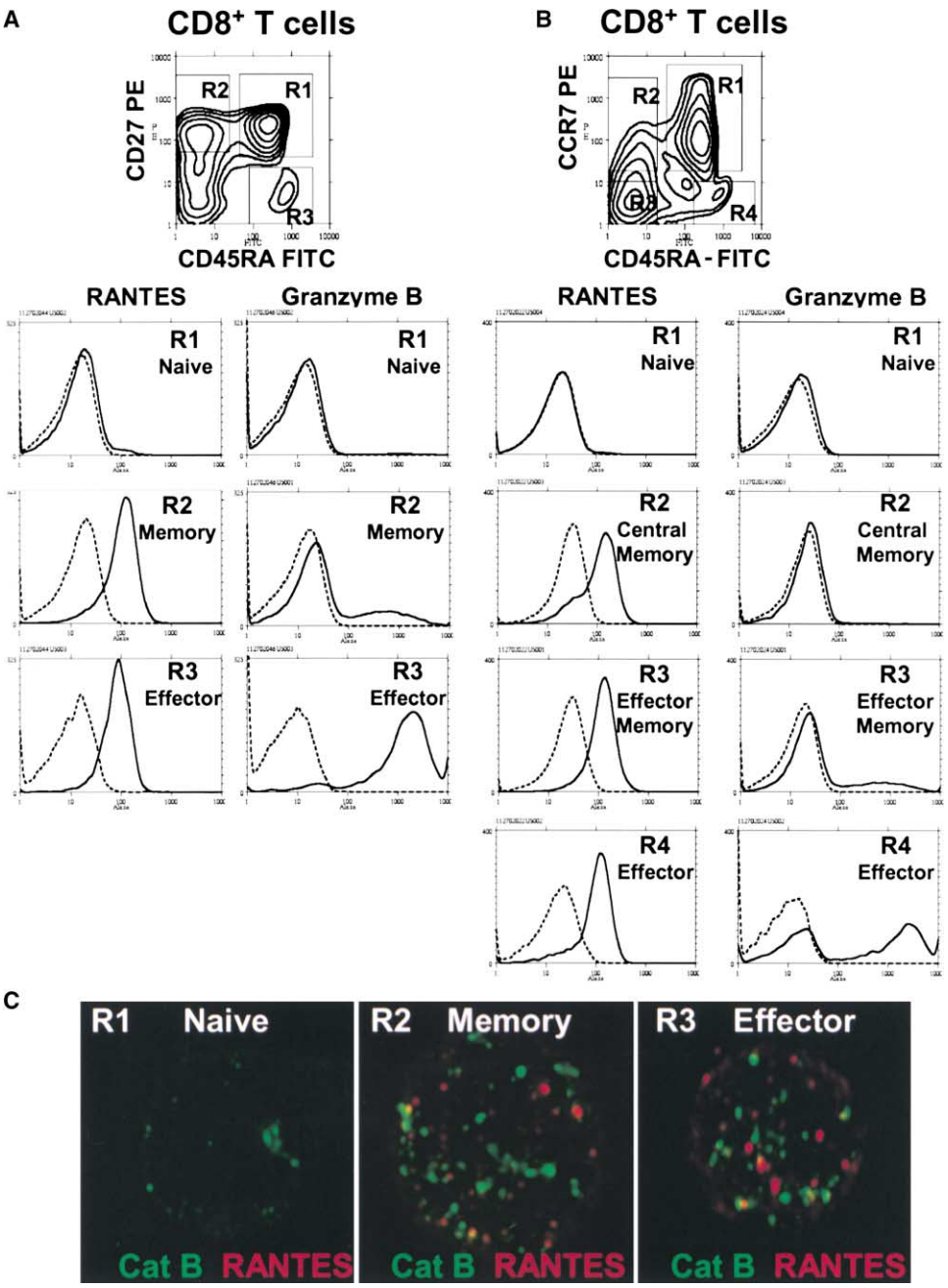

Figure 3. Memory and Effector Phenotype CD8$^+$ T Cells Express Intracellular RANTES

(A) Four color flow cytometry of purified CD8$^+$ T cells isolated from peripheral blood, surface stained for CD8, fixed, permeabilized, and then stained for RANTES or granzyme B. Gated CD8$^+$ T cells are shown. Dotted lines show isotope controls.

(B) Similar experiment phenotyping CD8+ T cells by CD45RA and CCR7 expression.

(C) Fluorescence microscopy of permeabilized blood CD8$^+$ T cells purified by flow cytometry based on surface staining for CD45RA/CD27 as in (A). Merged whole-cell images were reconstructed after processing by deconvolution microscopy. RANTES is shown in red, and the lysosomal antigen cathepsin B in green. Image processing was identical for all images, and control primary antibody staining for these markers appeared black under these conditions.

this lysosomal enzyme, which was also generally symmetrically distributed in vesicles throughout the cytoplasm.

Due to the limited numbers of purified subpopulations of CD8$^+$ blood T cells (especially the effector subpopulation), we examined the intracellular RANTES localization in short-term in vitro-activated CD8+ T cell blasts. These highly active in vitro cytotoxic effector cells (data not shown) were expected to be more similar to cloned CD8+ CTL lines. CD8$^+$ T cell blasts showed a similar pattern of RANTES staining to that found in memory and effector blood CD8+ T cells, with a greater number of positive vesicles and somewhat more intense staining (Figure 4). In order to characterize the intracellular com-

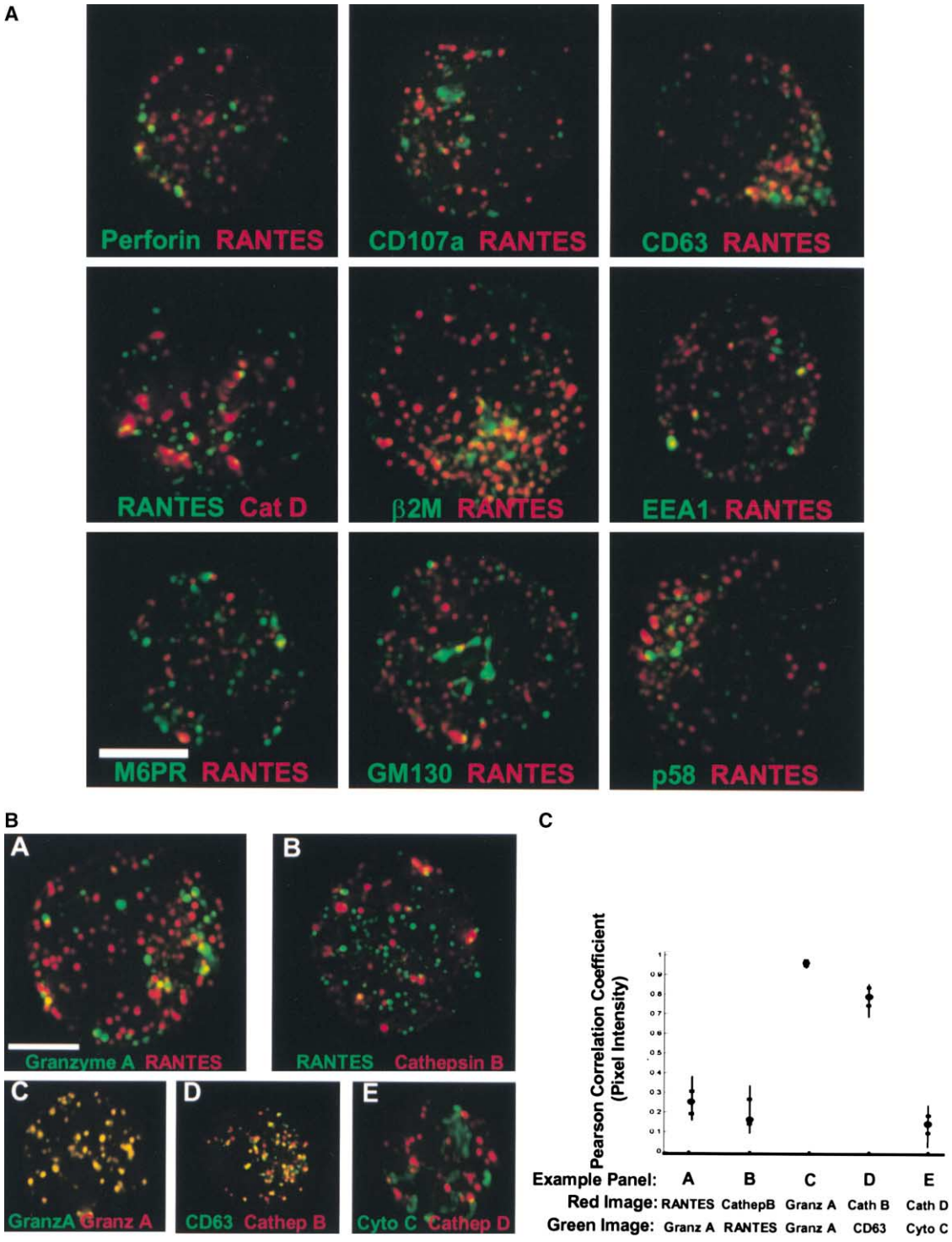

Figure 4. Costaining of Intracellular RANTES with Intracellular Markers in CD8$^+$ T Cell Blasts

(A) Merged two color images of 3D reconstruction of deconvolved digital images of permeabilized CD8$^+$ blasts stained with antibodies against perforin, CD107a, CD63, β2-microglobulin EEA1, M6PR, GM130, and p58 (green) combined with RANTES (red). For the cathepsin D stain, RANTES costaining is in green.

(B) Deconvolution and 3D analysis for images were performed with CD8$^+$ T cell blasts stained for A, granzyme A (green) and RANTES (red); B, RANTES (green) and cathepsin B (red); C, postive controls: granzyme A staining (red and green); and D, lysosome proteins CD63 (green) and cathepsin D (red); E, negative control: cytochrome c (green) and cathepsin D (red).

(C) Statistical analysis of two color pixel intensity correlation in all optical sections in ten cells as expressed by Pearson correlation coefficient. Points show the mean correlation coefficient for all sections, bars show total range, hatch marks indicate first and third quartiles. Scale bar, 3.5 μm.

partment in which RANTES is expressed, costaining was carried out with a variety of markers for cytotoxic mediators (perforin, granzyme A), lysosomal markers (CD107a, CD63, cathepsins B and D), and markers for other cytoplasmic organelles, such as endosomes (EEA1 and mannose-6-phosphate receptor) and Golgi (GM130 and p58). In addition, we stained intracellular β2-microglobulin as a marker of the constitutive secretory pathway. In all these cases, there was minimal colocalization of RANTES and the second marker, with a maximum of only a small percentage of the RANTES stain expressed in the same region as the second marker.

Because the lack of colocalization with cytotoxic mediators and lysosomal markers was unexpected in view of the previous findings with CTL clones (Wagner et al., 1998), we further investigated whether the minimal RANTES colocalization observed with cytotoxic and lysosomal markers was significant. For each combination shown in Figure 4B, the two color digital images of all optical planes in ten cells were quantitatively analyzed as described in the Experimental Procedures section and the Pearson correlation coefficients calculated for the two colors.

As positive controls for colocalization, we analyzed the staining with a primary granzyme A mAb followed by a mixture of secondary anti-Ig labeled with different fluorophores (Figures 4B and 4C) and also staining of the two lysosomal markers CD63 and cathepsin B (Figures 4B–4D). Both of these showed extensive colocalization visually as expected, although the latter showed some distinct compartments for each marker. As a negative control for colocalization, we stained for the mitochondrial protein cytochrome c and the lysosomal marker cathepsin D (Figures 4B–4E), and these markers visually showed minimal colocalization. The quantitative statistical analysis of pixel intensities (Figure 4C) showed that the correlation of pixel intensities of the two stains was excellent for the positive controls (Pearson correlation coefficient, $r > 0.75$) and very weak for the negative control ($r \sim 0.15$). For the combinations of RANTES, granzyme A, and cathepsin B, the correlation was also weak ($r \sim 0.17$–0.25) and overlapped the negative control, demonstrating that RANTES colocalization with lysosomal granule markers was not significantly different from the negative control. This analysis cannot rule out a small level of colocalization of RANTES and the secretory lysosomal granule markers but suggests that much of the apparent minor degree of colocalization seen visually may be due to inadequate spatial resolution of current optical techniques.

Subcellular Localization of RANTES$^+$ in T Cell Blasts by Electron Microscopy

Since fluorescence microscopy does not resolve the ultrastructure of the small RANTES-containing organelles, we used the sensitive technique of ultrathin cryosectioning and immunogold labeling in order to obtain high-resolution EM images. Analysis of CD8$^+$ T blasts with anti-RANTES antibodies revealed a clear vesicular labeling pattern. The positive vesicular structures were between 80 and 180 nm in size, contained a limiting membrane, and had electron-lucent (nongranular) contents (Figure 5). The nucleus, cytosol, mitochondria, and plasma membrane did not label, indicating the specificity of the antibody. Low levels of label were also seen in Golgi (Figure 5 and Supplemental Figure S1, arrowheads, at http://www.immunity.com/cgi/content/full/20/2/219/DC1), demonstrating the biosynthetic origin. Plasma membrane and clathrin-coated pits and vesicles (Figure 5) did not label, suggesting minimal recycling of RANTES via the plasma membrane. Label in electron-dense cytolytic granules (about 350 nm in size) was mostly absent and only observed occasionally. From these data we conclude that RANTES is localized in vesicular structures that are distinct from and smaller in size than the characteristic T cell granules. We propose the name RANTES storage vesicles (RSV) for these vesicles.

RANTES$^+$ Secretory Vesicles Are Mobilized Quickly after TcR Crosslinking

In order to gain insights into the early TcR-induced secretion of RANTES versus the exocytosis of granules, T cell blasts were triggered with beads coated with anti-CD3/CD28, fixed after various incubation times, and their granules examined by confocal microscopy. Such beads adhered readily to T cells and induced RANTES and β-hexosaminidase secretion comparable to the coated wells used above. Control beads coated with IgG had much less tendency to adhere to T cells and did not induce granule polarization or RANTES secretion in CD4$^+$ and CD8$^+$ T cells (data not shown). Figure 6A shows a z series of confocal images of CD8$^+$ T cell blasts after 5 or 40 min of incubation with anti-CD3/CD28 and stained for RANTES (red) and granzyme A (green). At 5 min, RANTES staining was significantly polarized toward the activating bead, while granzyme A appeared somewhat less polarized. As was the case with resting cells, some colocalization of these markers was seen, but there was no clear increase in the degree of colocalization with time after TcR stimulation (as reported in CTL clones; Wagner et al., 1998). The level of RANTES staining was diminished at 5 min compared to unstimulated cells or those fixed after 1 min, and after 40 min, RANTES staining was close to background levels (Figure 6A). This observation shows that even with new protein synthesis occurring, the RSV are depleted after TcR ligation. Granzyme A staining was highly polarized after 40 min, with only a small decrease in intensity compared to unstimulated cells. In experiments in which RANTES was costained with the lysosomal markers cathepsin D and CD107b, the latter behaved similarly to granzyme A (data not shown).

To compare RANTES and granzyme A secretion as measured by loss of their intracellular content to measurements of supernatant release (Figures 1 and 2), we quantitated the TcR-triggered decrease in fluorescent staining by flow cytometry in the presence of cycloheximide. As shown in Figure 6B, RANTES staining decreases rapidly, with a burst of loss over the first 30 min (half decay time of half decay time of 10 min) and then plateaus to a level of 30%–40% of the original. In contrast, granzyme A decreases more slowly in both subsets, with levels of 70%–80% of the original still present after 1 hr.

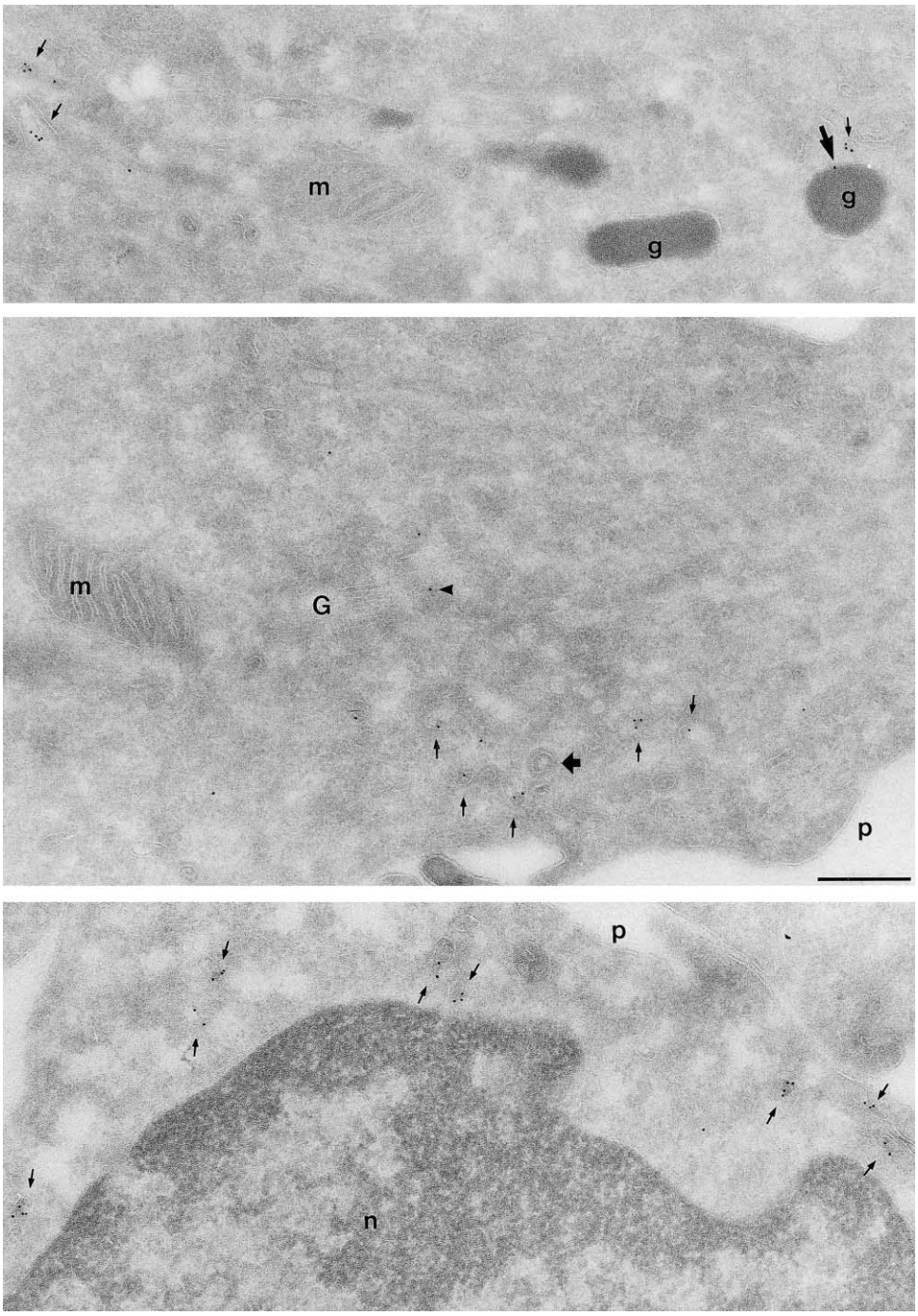

Figure 5. RANTES Is Stored in Specialized Storage Vesicles Distinct from the Electron-Dense Granules

The subcellular localization of RANTES in T cell blasts was performed with the cryo-immunogold EM technique. Ultrathin cryosections of $CD8^+$ T blast were labeled with anti-RANTES antibodies. Anti-RANTES is visualized with 10 nm gold particles and localized in 80–180 nm diameter vesicles that contain a limiting membrane (small arrows). Golgi (G) contained occasional gold label (arrowhead, middle panel). Granules (g) were rarely labeled (bold arrow in upper panel). The plasma membrane (p) and clathrin-coated pits and vesicles (thick arrow in middle panel) were not labeled. Mitochondria (m), nucleus (n), and cytosol served as background control and were not labeled. Scale bar, 200 nm (applies to all panels).

Discussion

Early TcR-Induced RANTES Secretion Occurs by a Regulated Secretory Pathway

Examination of activation-induced chemokine secretion by CD8+ T cells revealed a remarkably rapid release of RANTES into supernatants from memory and effector phenotype blood cells and blasts, characterized by a burst of secretion plateauing after 30–60 min of stimulation (Figures 1 and 2). Cycloheximide or brefeldin A pretreatment had no significant effect on this rapid burst of RANTES secretion, although in blasts these blockers

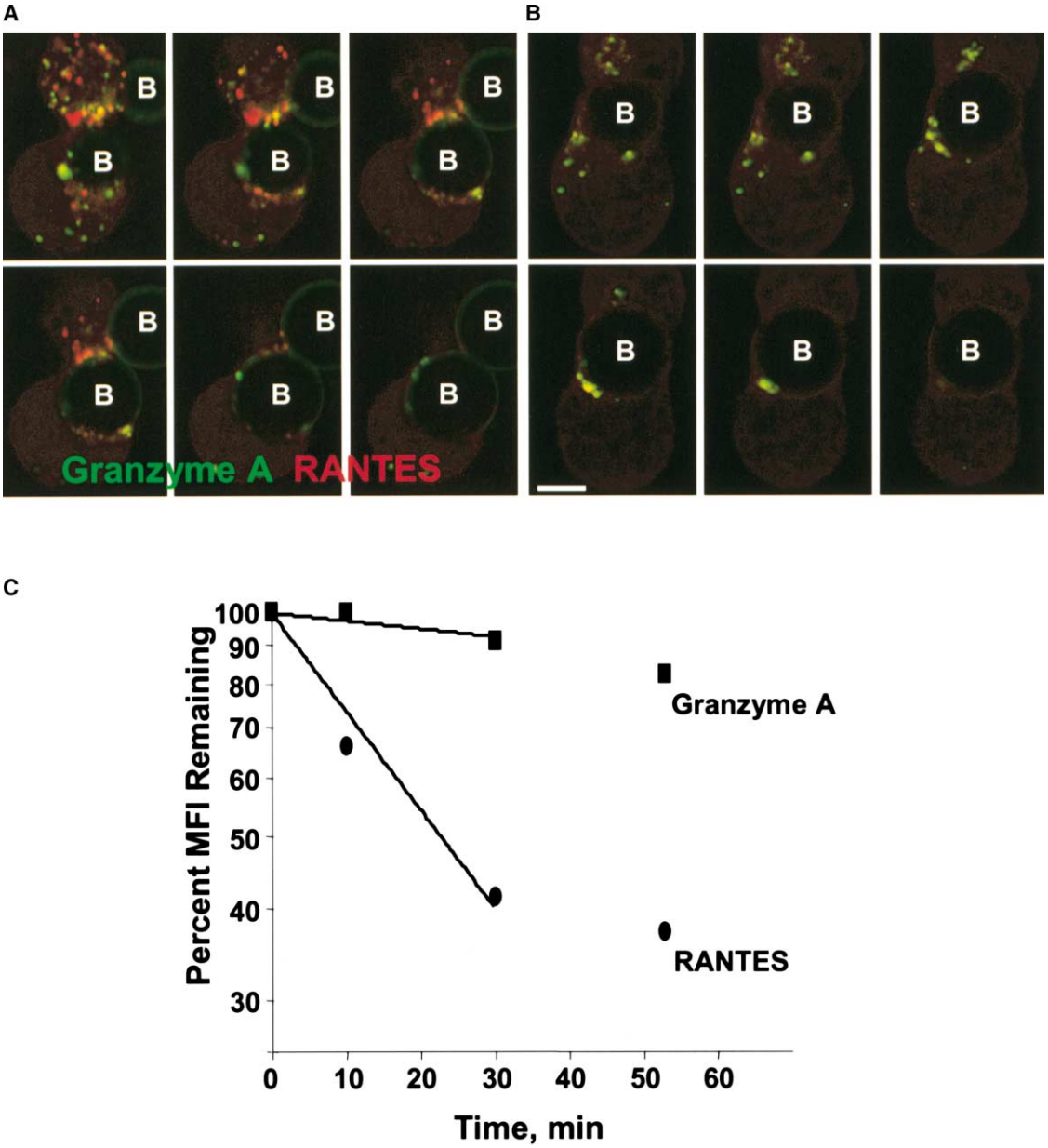

Figure 6. Polarization and Depletion of Intracellular RANTES after TcR Crosslinking

Purified CD8$^+$ T cell blasts were incubated for 5 (A) or 40 (B) min with beads coated with mAbs against CD3 and CD28 (cell/bead ratio, 2). After incubation, cell suspensions were fixed, permeabilized, and stained for RANTES (red) and for granzyme A (green), followed by confocal microscopy. Six planes of a z series (beginning from upper left to bottom right) are shown. Beads bound to the T cells are indicated by (B). Scale bar, 3 μm. (C) CD8$^+$ T cell blasts were stimulated with anti-CD3/anti-CD28 mAbs immobilized on the well surface in the presence of cycloheximide for the indicated times, followed by harvest and fixation. After permeabilization, the cells were stained with anti-RANTES-PE (ovals) and anti-granzyme A-FITC (rectangles) and analyzed by flow cytometry. This semilog plot shows the mean fluorescence intensities at each time expressed as a percentage of the initial value. The lines show least mean square fitted first order decay curves for the first 30 min.

of new protein synthesis gave substantial inhibition at later times (Figure 2). Secretion of the chemokines MIP-1α and MIP-1β and of interferon-γ was detectable only after several hours of activation, showed a lag at early times, and was effectively blocked by cycloheximide and brefeldin A. In CD8$^+$ blasts, secretion of the lysosomal enzyme β-hexosaminidase was followed as a measure of granule exocytosis. Like RANTES, this secretion was not inhibited by cycloheximide and brefeldin A, but its release kinetics was slower than RANTES and plateaued only after 4 to 5 hr (Figure 2 and data not shown). Another difference between RANTES secretion and degranulation became apparent when both supernatant and cell-associated RANTES were measured. We found that within 1.5 hr after activation, 60% of the RANTES detectable in lysates had been secreted, while, at this time, less than 15% of the total β-hexosaminidase had been released into the supernatant. Thus, activation

rapidly releases a higher proportion of intracellular RANTES than of this granule marker. These observations are consistent with the substantial loss in RANTES vesicular staining seen between 5 and 40 min (Figure 6A) and also with the rapid decrease of intracellular RANTES by flow cytometry (Figure 6B). In contrast, the loss of intracellular granzyme A was much slower, both microscopically and as quantitated by flow cytometry. These results are difficult to reconcile with a simple model in which RANTES is stored in the same regulated secretory compartment as the cytotoxic mediators, but it remained possible that RANTES was selectively stored in a particularly mobilizable subpopulation of granules.

RANTES Is Stored Intracellularly in T Cells in a Distinct Secretory Compartment

Confocal fluorescence microscopy on permeabilized CD8+ T cell blasts showed that the great majority of RANTES stain did not colocalize with granule components but by visual inspection we could find a small percentage of staining that did (data not shown). Because it seemed possible that this minor amount of colocalization was an artifact of the limited optical resolution of confocal microscopy when applied to the small lymphocyte cytoplasm, we carried out an extensive analysis of RANTES colocalization with a variety of markers using deconvolution fluorescence microscopy, which has superior three-dimensional spatial resolution (Figure 4). This approach showed very minor RANTES colocalization with granule markers, less than was seen with confocal microscopy. To test whether this minor degree of colocalization was significant, the quantitative analysis of pixel intensities was carried out (Figure 4C), which showed that the level of RANTES colocalization with granule markers was equivalent to the negative control of mitochondrial and lysosomal markers. The possibility that the RANTES-containing vesicles fuse with a mobilizable subfraction of cytotoxic granules after activation is very unlikely given the lack of increased colocalization after activation (Figure 6). Overall, these observations indicate that RANTES is not colocalized with the cytotoxic granules, which are the only known intracellular compartment known to undergo activation-induced exocytosis in T cells.

The possibility that intracellular RANTES is contained in elements of the constitutive secretory or endosomal pathways was tested by examining RANTES colocalization with respect to Golgi markers, endosomal markers, and intracellular β2-microglobulin as a marker for the constitutive secretory pathway, and minimal overlap was observed in all cases. Thus, it appears that RANTES is stored in memory and effector $CD8^+$ T cells intracellularly in a previously undescribed secretory compartment, which we have termed RANTES secretory vesicles (RSV).

Electron microscopy shows that RSV have a distinctly different morphology of RSV from the granules containing cytotoxic mediators. The latter are somewhat larger and have characteristic staining cores absent in RSV. The apparent similarity in size of RSV and the lysosomal granule by fluorescence microscopy could be explained by its inability to resolve a complex structure of closely spaced saccules, as was recently described for ER-to-Golgi carriers (Mironov et al., 2003). The finding of two distinct compartments containing stored secretory mediators is not unique to lymphocytes, although granule heterogeneity has not been previously described in CTL by EM studies (Peters et al., 1991). Neutrophils contain multiple subpopulations of secretory granules with differing mediator content and differing exocytosis rates after activation (Borregaard and Cowland, 1997). The gelatinase-positive tertiary granules are generally similar in size to lymphocyte RSV and are rapidly exocytosed compared to the larger lysosomal azurophilic granules. Eosinophils are particularly relevant to the present results, in that RANTES is been shown to be stored in both the cortex of the major lysosomal granules (containing major basic protein and eosinophil peroxidase) and in smaller vesicles with a lighter density (Lacy et al., 1999). After activation of eosinophils with interferon-γ, a substantial fraction of RANTES was secreted more rapidly than lysosomal granule markers, with concomitant depletion of the lighter RANTES-containing vesicles. These findings parallel to a considerable extent our observations in T lymphocytes, although we find less RANTES associated with T cell granules. Our observations do not support a "piecemeal degranulation" mechanism in which RANTES is transferred from the major granules to vesicles that undergo activation-induced exocytosis. Our results are more consistent with a distinct second regulated secretory pathway, with the minor degree of RANTES association with lysosomal granules perhaps due to autophagy.

Our data that $CD8^+$ memory-phenotype T cells initially secrete stored RANTES contrasts with a recent report in which RANTES secretion by in vitro-generated mouse memory $CD8^+$ T cells was blocked by cycloheximide at 3 hr after activation (Swanson et al., 2002). Intracellular RANTES was also undetectable by fluorescence microscopy in these cells. Although we find that RANTES secretion from human blood memory phenotype cells remains independent of protein synthesis for several hours, at later times newly synthesized protein dominates RANTES secretion (data not shown). We would speculate that the in vitro-generated mouse memory $CD8^+$ cells are different from memory cells isolated directly ex vivo and that detection of intracellular mouse RANTES by immunofluorescence may be less sensitive than is the case with the human system. Another recent report on RANTES secretion in mouse memory CD8+ T cells did show early cycloheximide-resistant RANTES secretion that was overwhelmed by cycloheximide-sensitive RANTES production within 2 hr (Walzer et al., 2003). These results are compatible with our findings in the human system, where we find that RANTES secretion by $CD8^+$ blasts cells increases greatly several hours after stimulation, where newly synthesized protein dominates secretion.

Our results suggest that a regulated secretion pathway may be an important mechanism used by $CD8^+$ T cells to secrete noncytotoxic effector molecules and that this mechanism may be particularly important early after antigen recognition. Rapid RANTES release may provide a critical positive feedback loop to enhance

inflammation after the initial recognition of antigen by effector T cells. It is well accepted that chemokines are important mediators regulating leukocyte trafficking (Sallusto et al., 2000), and this rapid T cell chemokine secretion may add to the chemokines released by tissue cells themselves after injury. Another function of β chemokines is their ability to promote T cell activation. RANTES was shown to rapidly induce T cell degranulation directly, and to enhance cytotoxicity via the granule exocytosis pathway (Taub et al., 1996). Thus, early release RANTES secretion may enhance the slower release of the granules containing perforin and granzymes, thus providing another kind of positive feedback to the degranulation process. Thus, it would appear that rapid secretion of chemokines, such as RANTES, can enhance T cell activation via several independent mechanisms and may play potentially critical roles in controlling immune responses in vivo.

Experimental Procedures

T Cells

PBMC were obtained from lymphocyte apheresis preparations from NIH blood bank normal healthy donors. After purification by Ficoll-paque gradients (Amershan Pharmacia Biotech, Sweden), $CD8^+$ T cells were purified by negative selection using CD8-magnetic beads (Miltenyi Biotec, Auburn, CA). Naive, memory, and effector $CD8^+$ T cell subsets were sorted by flow cytometry after surface staining with CD45RA-FITC, CD27-PE, CD8-APC, and the subfractions culture experiments or analyzed by fluorescence microscopy.

For in vitro-activated $CD8^+$ T cells, PBMC were cultured in RPMI supplemented with 10% FCS, antibiotics, and nonessential amino acids, in the presence of 2.5 μg/ml of PHA (Sigma-Aldrich, St Louis, MO) and 20 U/ml of rIL-2 for 10 days. In some experiments, PBMC were expanded by allogeneic stimulation with irradiated HLA mismatched donors (2:1 responder to stimulator ratio) rather than PHA. Similar results were obtained with both blast preparations. $CD8^+$ T cells were purified as above. After purification, these cells were maintained in culture medium with 20 U/ml of rIL-2, at least for 3 days before experiments. Subpopulation purity, tested by flow cytometry using CD4-PE and CD8-FITC (BD Pharmingen, San Jose, CA), was >90%.

Degranulation

Purified $CD8^+$ T cells blasts were resuspended in degranulation buffer (HBSS + 1 mg/ml BSA) at 1×10^7 cell/ml. Aliquots were treated either with medium, 7.5 μg/ml cycloheximide (CHX), or 5 μg/ml Brefeldin A (BFA) (both reagents from Sigma-Aldrich, St Louis, MO). After 1 hr at 37°C, cells were washed once with degranulation buffer and adjusted to 3×10^6 cells/ml with new drug added. Degranulation was stimulated by PMA 20 ng/ml and Ionomycin 1 μM. In some experiments, TcR stimulation was induce using precoated plates with 10 μg/ml of anti-CD3 (clone UCHT1) and 5 μg/ml anti-CD28 (clone CD8.2, BD Pharmingen, San Jose, CA). The supernatants were harvested at different time points and kept at −20°C until tested. Total cell contents were obtained from extracts in 0.2% of Triton X-100.

Chemokines and IFN-γ Assays

Secretion of MIP-1α (CCL3), MIP-1β (CCL4), RANTES (CCL5), and IFN-γ were measured by ELISA assays of supernatants (R&D Systems, Inc., Mineapolis, MN). ELISA plates were coated overnight with 4 μg/ml of the capture mAbs diluted in PBS, washed in PBS + 0.05% Tween-20, and blocked for 1 hr with blocking buffer (PBS + 1% BSA + 5% sucrose + 0.05% NaN_3). Supernatants from the stimulation protocol and diluted Triton lysates were incubated for 2 hr, washed, and the plates incubated with biotinylated detection antibodies for 2 hr. After washing, wells were incubated for 1 hr with 0.5 μg/ml streptavidin-coupled HRP (Molecular Probes, Inc., Eugene, OR). The plates were developed with ABTS solution (Southern Biotechnology Associates, Inc, Birmingham, AL) and the absorbance at 405 nm read using a Victor plate reader.

β-Hexosaminidase Assay

β-hexosaminidase activity was measured by incubation of 100 μl of supernatant with 100 μl of 1 mM methylumbelliferyl-N-acetyl-β-glucosaminide (Sigma-Aldrich, St. Louis, MO), in 0.2% Triton X-100 + 0.25 M citrate (pH 4.8). After 1 hr at 37°C, the fluorescence (ex355/em460 nm) was measured in a Victor reader plate (Wallac OY, Finland). Secretion was calculated as supernatant enzyme activity expressed as a percentage of total cell enzyme activity assayed in a Triton extract.

Flow Cytometry

Internal RANTES and granzyme B content was analyzed by flow cytometry of fixed and permeabilized cells that were first stained for surface phenotype. Purified $CD8^+$ T cells (1×10^6) were initially stained using anti-CD45RA-FITC, anti-CD8-APC (Caltag, Burlingame, CA), and anti-CD27-PE (Pharmingen, San Jose, CA). Alternatively, cells were stained with anti-CCR7 (eBioscience, San Diego, CA) followed by goat anti-mouse-PE, then with unlabeled mouse IgG, before staining with CD45RA-FITC and CD8-APC. After surface staining, fixation with paraformaldehyde and permeabilization saponin using Cytofix/Cytoperm (Pharmingen) was performed. Internal staining utilized anti-RANTES-biotin or anti-granzyme B-biotin (Caltag, Burlingame, CA) followed by streptavidin-Alexa 594 (Molecular Probes, Eugene, OR) and was analyzed with a FACScan.

Decrease of mean fluorescence intensity of RANTES and granzyme A was measured after TcR stimulation by flow cytometry. $CD8^+$ T cell blasts were treated with CHX for 1 hr. After treatment, $CD8^+$ T cells were triggered by mAbs anti-CD3/anti-CD28-coated plate for the indicated times in the presence of CHX. At these time points, cells were harvested and stained with monoclonal anti-RANTES-PE, anti-granzyme A-FITC, and negative control isotypes IgG-PE and IgG-FITC, respectively (BD Pharmingen, San Jose, CA). TcR-induced intracellular depletion of secreted markers was analyzed by flow cytometry and calculated for each marker relative to its mean fluorescence intensity at time zero.

Confocal Microscopy

T cells were stimulated by bead-bound antibody, prepared by incubating 6 μm polystyrene beads (Polysciences, Inc. Warrington, PA) overnight with 10 μg ml^{-1} anti-CD3 and 5 μg ml^{-1} anti-CD28 mAbs in 0.1 M borate buffer (pH 8.5) followed by washing. Purified $CD8^+$ T cells were mixed with coated beads at 2:1 cell:bead ratio and centrifuged at 500 rpm for 5 min to allow conjugate formation. After centrifugation, pellets were resuspended and incubated at 37°C for 5 or 40 min, fixed in suspension with 2% paraformaldehyde in PBS, washed with HBSS, and plated on coverslips precoated with poly-L-lysine. After adherence, the coverslips were washed with PBS and further fixed for 30 min with 4% paraformaldehyde, followed by two quenching steps of 5 min each with 50 mM of NH_4Cl. Cells were permeabilized with 1% NP-40 in wash buffer (PBS + 3% FCS + 0.01% saponin) for 10 min. The cells were labeled with granzyme A mAb (BD Pharmingen, San Jose, CA) followed by Alexa-488-rabbit anti-mouse IgG and biotinylated goat anti-RANTES (R&D Systems, Inc) followed by Alexa 568-donkey anti-goat IgG. Secondary antibodies all came from Molecular Probes. After staining, the coverslips were mounted with Prolong antifade (Molecular Probes). Samples were examined with a Zeiss LSM510 confocal microscope.

Deconvolution and Colocalization Analysis

Purified $CD8^+$ T cell blasts were fixed and permeabilized as above and then stained with perforin and M6PR mAbs (RDI, Flanders, NJ), granzyme A mAb (BD Pharmingen, San Jose, CA), EEA1 and GM130 mAbs (BD Transduction Laboratories, San Jose, CA), p58 mAb (Sigma-Aldrich, St. Louis, MO), and β2-microglobulin mAb (BD Pharmingen), all followed by Alexa 488-rabbit anti-mouse IgG, FITC-CD107a, and FITC-CD63 mAbs (BD Pharmingen, CA), followed by Alexa 488-rabbit anti-fluorescein, rabbit anti-cathepsin B (Athens Research & Technology, Athens, GA), followed by Alexa 488-donkey

anti-rabbit IgG. This staining was combined with biotinylated goat anti-RANTES followed by Alexa 568-labeled donkey anti-goat IgG. In some experiments (images with RANTES shown in green), rabbit anti-cathepsin D (DAKO, CA) or rabbit anti-cathepsin B were detected with Alexa 568-goat anti-rabbit IgG, in combination with biotinylated goat anti-RANTES followed by Alexa 488-mouse anti-biotin. Controls performed by staining with the secondary antibodies using purified isotype-matched IgG in all cases showed negligible staining. Cells were imaged with an inverted fluorescence microscope (Model IX70, Olympus America, Inc) using a 1.35 NA 100× objective; FITC, rhodamine, and Cy5 filter sets; and a Photometrics CH350 12-bit camera (Photometrics) with a KAF 1400 chip on a DeltaVision imaging system (Applied Precision). Images were acquired and analyzed with a UNIX-based Silicon Graphics O2 workstation with SoftWoRx software installed. For imaging with the 100× objective, camera wells were not binned, leading to a pixel size of 0.07 μm in *x* and *y*. *z* steps were set to 0.07 μm, yielding cubic voxels. The typical xyz image size was 256 × 256 × 100. These images were deconvolved using the deconvolve command with the default settings for this constrained iterative algorithm in the SoftWoRx software. Chromatic aberration between the red and green channels was measured using multicolor fluorescent beads. A shift of 0.07 μm was detected in *z*, so green images were routinely shifted relative to red images by this amount.

Deconvolved images corrected for chromatic aberrations were analyzed for colocalization in 3D. The amount of colocalization between the deconvolved and corrected red and green images was estimated by computing the Pearson coefficient (Manders et al., 1993). This number gives an overall estimation of the three-dimensional spatial correlation between both stains on a pixel basis, with a maximum value of one. As a first approximation, this number can be used to represent the fractional amount of colocalization between fluorescein and rhodamine in any given regions of the image. The region of interest was defined automatically with an isodata threshold followed by a convex hull algorithm to segment the cell. The operator visually checked that these boundaries were satisfactory and with manual entry as an alternative. The Pearson coefficient is a robust estimator of colocalization since it is background, noise, and intensity independent. The colocalization analysis as well as the statistical analysis (ANOVA tests) was performed on the Matlab platform (MathWorks Inc., Natik, MA) and DIPimage (image processing toolbox for Matlab, Delft University of Technology, The Netherlands).

For each marker comparison, 10 to 11 cells were analyzed, each using 100 images of planes spaced at 0.069 μm. The following antibodies were used as positive and negative controls for colocalization. Positive controls: (1) anti-granzyme A mAb (BD Pharmingen, San Jose, CA), followed by the secondaries Alexa 488 and Alexa 568 rabbit anti-mouse; (2) FITC-anti-CD63 (BD Pharmingen, San Jose, CA) followed by Alexa 488-goat anti-fluorescein and rabbit anti-cathepsin B (DAKO, CA) followed by Alexa 568-goat anti-rabbit. Negative control: cytochrome c mAb (BD Pharmingen, San Jose, CA) followed by Alexa 488-goat anti-mouse and rabbit anti-cathepsin D (DAKO, CA), followed by Alexa 568-goat anti-rabbit. RANTES was detected as above. All secondary antibodies were from Molecular Probes, OR.

Electron Microscopy

Fixation was performed by adding an equal volume of 4% paraformaldehyde and 0.4% glutaraldehyde in PHEM buffer to the warm culture medium that contained the T cells. Fixed cells were collected, embedded, and processed for cryosectioning with a Leica FCS as described previously (Peters and Hunziker, 2001). Samples were trimmed using a diamond Cryotrim 90° knife at −100°C (Diatome, Switzerland) and ultrathin sections of 50 nm were cut at −120°C using an ultramicrotome cryo-immuno 35° knife (Diatome, Switzerland). Immunogold labeling was performed using biotinylated goat anti-RANTES antibody as above, with detection by protein-A conjugated to 10 nm gold (EM laboratory, Utrecht University). Sections were studied using a Philips CM10 transmission electron microscope (Peters and Hunziker, 2001).

Acknowledgments

We thank Dr. Michael Kruhlak for help with confocal microscopy; Larry Granger and Sue Sharrow for help with flow cytometry; and Dr. Paul Roche for helpful comments.

Received: November 14, 2003
Revised: January 14, 2004
Accepted: January 20, 2004
Published: February 17, 2004

References

Borregaard, N., and Cowland, J.B. (1997). Granules of the human neutrophilic polymorphonuclear leukocyte. Blood *89*, 3503–3521.

Conlon, K., Lloyd, A., Chattopadhyay, U., Lukacs, N., Kunkel, S., Schall, T., Taub, D., Morimoto, C., Osborne, J., Oppenheim, J., et al. (1995). CD8+ and CD45RA+ human peripheral blood lymphocytes are potent sources of macrophage inflammatory protein 1 alpha, interleukin-8 and RANTES. Eur. J. Immunol. *25*, 751–756.

Fortier, A.H., Nacy, C.A., and Sitkovsky, M.V. (1989). Similar molecular requirements for antigen receptor-triggered secretion of interferon and granule enzymes by cytolytic T lymphocytes. Cell. Immunol. *124*, 64–76.

Greenberg, A.H., Khalil, N., Pohajdak, B., Talgoy, M., Henkart, P., and Orr, F.W. (1986). NK-leukocyte chemotactic factor (NK-LCF): a large granular lymphocyte (LGL) granule-associated chemotactic factor. J. Immunol. *137*, 3224–3230.

Henkart, P.A. (1994). Lymphocyte-mediated cytotoxicity: two pathways and multiple effector molecules. Immunity *1*, 343–346.

Kelly, R.B. (1985). Pathways of protein secretion in eukaryotes. Science *230*, 25–32.

Lacy, P., Mahmudi-Azer, S., Bablitz, B., Hagen, S.C., Velazquez, J.R., Man, S.F., and Moqbel, R. (1999). Rapid mobilization of intracellularly stored RANTES in response to interferon-gamma in human eosinophils. Blood *94*, 23–32.

Manders, E.M., Verbeek, F.J., and Aten, J.A. (1993). Measurement of colocalization of objects in dual-color confocal images. J. Microsc. *169*, 375–382.

Mironov, A.A., Mironov, A.A., Jr., Beznoussenko, G.V., Trucco, A., Lupetti, P., Smith, J.D., Geerts, W.J., Koster, A.J., Burger, K.N., Martone, M.E., et al. (2003). ER-to-Golgi carriers arise through direct en bloc protrusion and multistage maturation of specialized ER exit domains. Dev. Cell *5*, 583–594.

Peters, P.J., and Hunziker, W. (2001). Subcellular localization of Rab17 by cryo-immunogold electron microscopy in epithelial cells grown on polycarbonate filters. Methods Enzymol. *329*, 210–225.

Peters, P.J., Borst, J., Oorschot, V., Fukuda, M., Krähenbühl, O., Tschopp, J., Slot, J.W., and Geuze, H.J. (1991). Cytotoxic T lymphocyte granules are secretory lysosomes, containing both perforin and granzymes. J. Exp. Med. *173*, 1099–1109.

Robinson, E., Keystone, E.C., Schall, T.J., Gillett, N., and Fish, E.N. (1995). Chemokine expression in rheumatoid arthritis (RA): evidence of RANTES and macrophage inflammatory protein (MIP)-1 beta production by synovial T cells. Clin. Exp. Immunol. *101*, 398–407.

Sallusto, F., Lenig, D., Forster, R., Lipp, M., and Lanzavecchia, A. (1999). Two subsets of memory T lymphocytes with distinct homing potentials and effector functions. Nature *401*, 708–712.

Sallusto, F., Mackay, C.R., and Lanzavecchia, A. (2000). The role of chemokine receptors in primary, effector, and memory immune responses. Annu. Rev. Immunol. *18*, 593–620.

Swanson, B.J., Murakami, M., Mitchell, T.C., Kappler, J., and Marrack, P. (2002). RANTES production by memory phenotype T cells is controlled by a posttranscriptional, TCR-dependent process. Immunity *17*, 605–615.

Taub, D.D., Ortaldo, J.R., Turcovski-Corrales, S.M., Key, M.L., Longo, D.L., and Murphy, W.J. (1996). Beta chemokines costimulate lymphocyte cytolysis, proliferation, and lymphokine production. J. Leukoc. Biol. *59*, 81–89.

Wagner, L., Yang, O.O., Garcia-Zepeda, E.A., Ge, Y., Kalams, S.A.,

Walker, B.D., Pasternack, M.S., and Luster, A.D. (1998). Beta-chemokines are released from HIV-1 specific cytolytic T cell granules complexed to proteoglycans. Nature *391*, 908–911.

Walzer, T., Marcais, A., Saltel, F., Bella, C., Jurdic, P., and Marvel, J. (2003). Immediate RANTES secretion by resting memory CD8 T cells following antigenic stimulation. J. Immunol. *170*, 1615–1619.

Winslow, C.M., and Austen, K.F. (1982). Enzymatic regulation of mast cell activation and secretion by adenylate cyclase and cyclic AMP-dependent protein kinases. Fed. Proc. *41*, 22–29.

Zlotnik, A., and Yoshie, O. (2000). Chemokines: a new classification system and their role in immunity. Immunity *12*, 121–127.